SDC OPEN

PHOTORECEPTOR INNER SEGMENT MORPHOLOGY IN BEST VITELLIFORM MACULAR DYSTROPHY

DREW SCOLES, MD, PHD,* YUSUFU N. SULAI, PHD,† ROBERT F. COOPER, PHD,‡ BRIAN P. HIGGINS, BS,† RYAN D. JOHNSON, BS,† JOSEPH CARROLL, PHD,†‡§¶ ALFREDO DUBRA, PHD,†‡§¶ KIMBERLY E. STEPIEN, MD†

Purpose: To characterize outer retina structure in best vitelliform macular dystrophy (BVMD) and to determine the effect of macular lesions on overlying and adjacent photoreceptors.

Methods: Five individuals with BVMD were followed prospectively with spectral domain optical coherence tomography and confocal and nonconfocal split-detector adaptive optics scanning light ophthalmoscopy (AOSLO). The AOSLO cone photoreceptor mosaic images were obtained within and around retinal lesions. Cone density was measured inside and outside lesions. In 2 subjects, densities were compared with published measurements acquired ~2.5 years before. One subject was imaged 3 times over a 5-month period.

Results: The AOSLO imaging demonstrated that photoreceptor morphology within BVMD retinal lesions was highly variable depending on the disease stage, with photoreceptor structure present even in advanced disease. The AOSLO imaging was repeatable even in severe disease over short-time and long-time intervals. Photoreceptor density was normal in retinal areas immediately adjacent to lesions and stable over ~2.5 years. Mobile disk-like structures possibly representing subretinal macrophages were also observed.

Conclusion: Combined confocal and nonconfocal split-detector AOSLO imaging reveals substantial variability within clinical lesions in all stages of BVMD. Longitudinal cellular photoreceptor imaging could prove a powerful tool for understanding disease progression and monitoring emerging therapeutic treatment response in inherited degenerations such as BVMD.

RETINA 37:741–748, 2017

Best vitelliform macular dystrophy (BVMD), also known as Best disease (OMIM 607854; *BEST1*), is an autosomal dominant macular degeneration of variable penetrance. The disorder is characterized by varying accumulation of yellowish vitelliform material that can evolve into atrophic, fibrotic appearing lesions.[1,2] Clinical vitelliform lesions of BVMD are usually restricted to the macula, although lesions have been reported at more eccentric locations.[3]

Mutations in the *BEST1* gene located on chromosome 11q13 encoding the protein bestophin-1 are known to cause BVMD and several other retinal degenerative diseases.[4,5] Bestrophin-1 has been localized to the basolateral membrane of the retinal pigment epithelium (RPE)[6] and is thought to function as a calcium-sensitive chloride channel while also influencing other channel functions.[7–9] Dysfunction of this channel can lead to the hallmark findings of BVMD, including an abnormal electrooculogram, an electrophysiological test that measures changes in the transepithelial potential across the RPE throughout the retina.[10] Electrooculogram often shows diminished light peak response in individuals with BVMD, even when no clinical features are evident.[11]

Limited histological studies of BVMD have found an abnormal accumulation of lipofuscin granules in the RPE of some donor eyes[12–14] with photoreceptor loss over areas of intact RPE.[12,15] These findings are in agreement with a knock-in mouse model of BVMD that also demonstrated subretinal deposits of unphagocystosed photoreceptor outer segments and lipofuscin granules.[16] Some authors have hypothesized that dysfunction of the RPE leads to accumulation of toxic materials, which in turn leads to degeneration of the overlying photoreceptors in BVMD.[12,15] Some studies have found structurally normal RPE in BVMD lesions, with the primary impact of BVMD appearing to be subretinal to photoreceptors themselves.[17]

Advanced retinal imaging techniques have given insight into the effects of *BEST1* mutations on outer retinal structures in BVMD. Optical coherence tomography (OCT) studies have localized the vitelliform material in BVMD to the subretinal space,[17–21] and some have shown increased thickening of the reflective band corresponding to photoreceptor outer segments.[17,18] Recently, Abramoff et al[22] demonstrated what appears to be outer segment photoreceptor elongation with light adaptation in areas of the macula outside retinal lesions in BVMD, which suggests photoreceptor dysfunction beyond clinically apparent lesions. However, multifocal electroretinogram irregularities correspond to involved lesion areas,[23] and quantitative fundus autofluorescence on patients with BVMD showed normal quantitative fundus autofluorescence in nonlesion areas, suggesting no increased lipofuscin levels outside observed retinal lesions.[24] Previously, confocal adaptive optics scanning light ophthalmoscopy (AOSLO) indicated that some photoreceptor structure persists over areas of Best lesions, and photoreceptor density is normal in areas adjacent to clinical lesions in BVMD.[21] This study uses a new imaging technique, nonconfocal split-detector AOSLO, to better delineate photoreceptor structure in BVMD. Additionally, we sought to analyze changes in the photoreceptor mosaic over time.

From the *Department of Biomedical Engineering, University of Rochester, Rochester, New York; †Department of Ophthalmology, Medical College of Wisconsin, Milwaukee, Wisconsin; ‡Department of Biomedical Engineering, Marquette University, Milwaukee, Wisconsin; §Department of Cell Biology, Neurobiology, and Anatomy, Medical College of Wisconsin, Milwaukee, Wisconsin; and ¶Department of Biophysics, Medical College of Wisconsin, Milwaukee, Wisconsin.

Research reported in this publication was supported by the National Eye Institute, the National Institute of General Medical Sciences, and the National Center for Advancing Translational Sciences of the National Institutes of Health under award numbers R01EY017607, P30EY001931, T32GM007356, and UL1TR001436. Additional support received from the Thomas M. Aaberg Sr. Retina Research Fund, the Gene and Ruth Posner Foundation, Foundation Fighting Blindness, RD & Linda Peters Foundation, the Glaucoma Research Foundation Catalyst for a Cure Initiative, and an unrestricted departmental grant from Research to Prevent Blindness (RPB). A. Dubra is the recipient of a Career Development Award from RPB. This investigation was conducted in a facility constructed with support from the Research Facilities Improvement Program, Grant number C06RR016511, from the National Center for Research Resources, National Institutes of Health.

Presented in part as a poster at the Association for Research in Vision and Ophthalmology Annual Meeting 2014, Orlando, FL, May 5, 2014.

None of the authors have any conflicting interests to disclose.

Supplemental digital content is available for this article. Direct URL citations appear in the printed text and are provided in the HTML and PDF versions of this article on the journal's Web site (www.retinajournal.com).

Reprint requests: Kimberly E. Stepien, MD, Eye Institute-Medical College of Wisconsin, 925 North 87th Street, Milwaukee, WI 53226; e-mail: kstepien@mcw.edu

Methods

Subjects

Research procedures followed the tenets of the Declaration of Helsinki and were approved by the institutional review board at the Children's Hospital of WI (CHW 07/77); 4 previously described family members[21] and 1 unrelated subject, all with identified mutation (p.Arg218Cys c.652C→T) in *BEST1*[25] and clinical findings consistent with BVMD, participated in this study after giving written consent. See Table 1 for further information about each subject. Axial length measurement (Zeiss IOL Master; Carl Zeiss Meditec, Dublin, CA), visual acuity testing, and fundus photography were performed at the time of research imaging in all subjects.

Spectral domain optical coherence tomography

Spectral domain optical coherence tomography line and volumetric scans were performed using the Cirrus HD-OCT (Carl Zeiss Meditec). The location of the fovea was determined using the fovea-finder function of the Cirrus HD-OCT, and marked on the line scan ophthalmoscope image. Additional high-density volumetric scans acquired using the Bioptigen spectral domain optical coherence tomography (Bioptigen Inc, Morrisville, NC) nominally covering 7 × 7 mm (1000 A-scans/B-scan, 250 B-scans) were used to create *en-face* OCT sections with custom software (Java, Oracle; Redwood City, CA).[26] *En-face* projections of the ellipsoid zone were generated to display the extent of BVMD lesions (Figures 1 and 2). Multiple horizontal and vertical macular B-scans nominally covering 7 mm (1000 A-scans/B-scan; Bioptigen) were registered and averaged to increase the signal-to-noise ratio. All OCT images are displayed on logarithmic intensity scale.

Table 1. Subject Demographics

Subject	Age, years	Sex	Lesion Type	Acuity, Snellen
KS_0325	53	M	Atrophic	OS, 20/80
KS_0589	61	F	Atrophic	OS, 20/50
KS_0599	53	F	Late vitelliruptive	OD, 20/30
KS_0600	18	M	Early vitelliform	OS, 20/20
KS_0601	20	F	Vitelliform with early vitelliruptive	OS, 20/20

F, female; M, male; OD, right eye; OS, left eye.

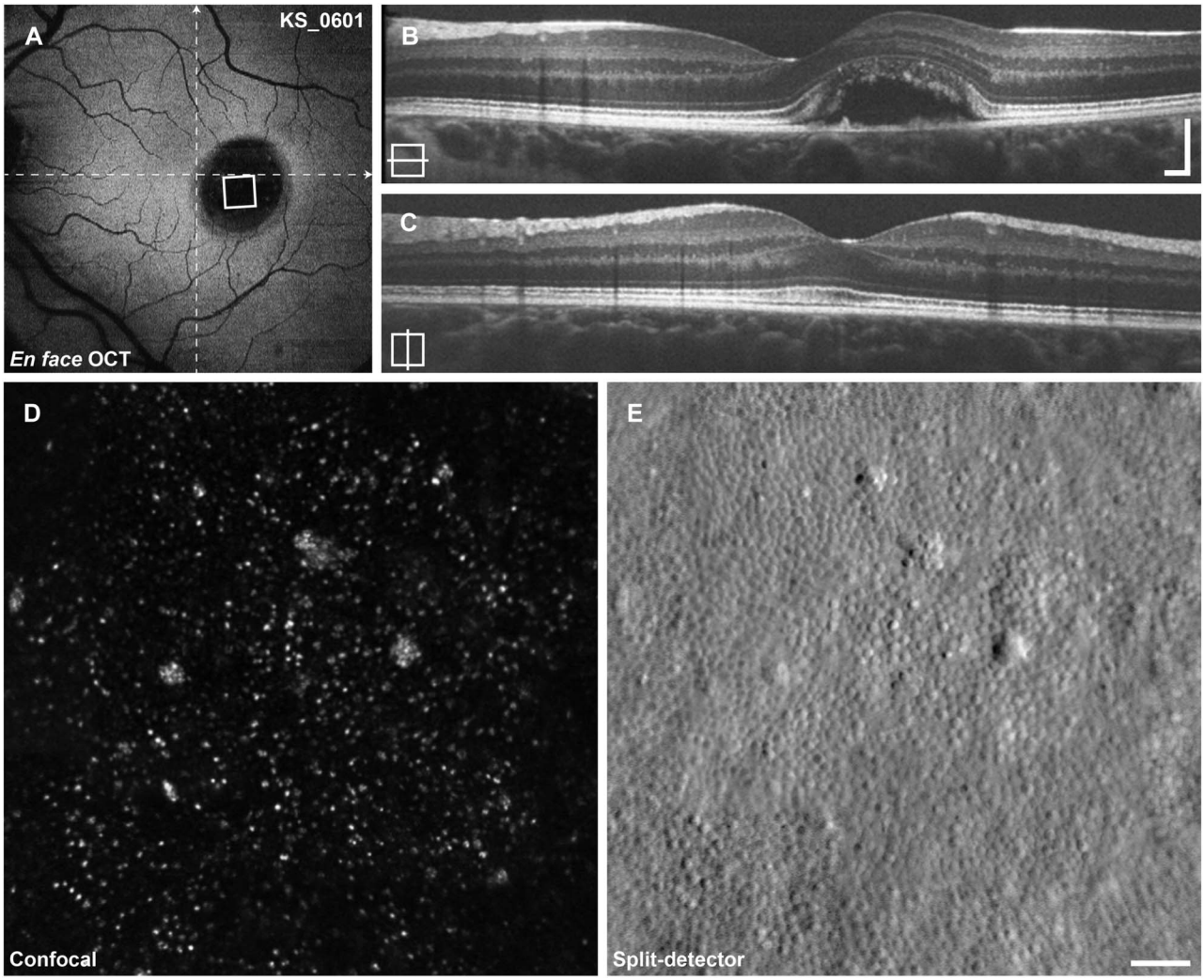

Fig. 1. Imaging results from subject KS_0601. **A.** *En-face* OCT at the level of the ellipsoid zone reveals a large ovoid retinal detachment at the location of the lesion. The area of AOSLO imaging shown below is indicated by the white square, dashed lines indicate the locations of the B-scans. **B** and **C.** Horizontal and vertical B-scan OCT reveals a large vitelliform lesion just nasal to the center of the fovea. **D.** Confocal AOSLO imaging reveals sparse photoreceptor reflectivity. **E.** The split-detector AOSLO imaging reveals a near-complete mosaic of cone photoreceptors. Cells identified in (**E**) show 1:1 correspondence to the sparse reflections seen in (**D**) with the exception of the large reflective clusters. Scale bars (**B** and **C**) 200 μm, (**D** and **E**) 50 μm.

Adaptive optics scanning light ophthalmoscopy

The AOSLO imaging was performed with a custom instrument, modified to capture light multiply scattered by the retina.[27] The multiply scattered light is divided spatially to two separate detectors, and the resulting images are then subtracted to form the nonconfocal split-detector image, which reveals the photoreceptor inner segment mosaic.[27] Confocal and split-detector images are recorded simultaneously in perfect spatial register. Photoreceptor image sequences were recorded at the fovea as well as in the periphery to approximately 10° superior and temporal to fixation. In subject KS_0589, an overlying epiretinal membrane in temporal macula obligated imaging to 10° nasal from fixation. Image sequences were corrected for sinusoidal distortion caused by the resonant scanner, then registered and averaged as previously described.[27] Using a simplified Gullstrand 2 schematic eye, the predicted 291 μm per degree of visual angle was scaled linearly by the subject's axial length to determine the scale of AOSLO images. Averaged AOSLO images were aligned manually in Adobe Photoshop (Adobe Systems Inc, San Jose, CA) to create a large montage. This montage was manually aligned to the color fundus, line scan ophthalmoscope, *en-face* OCT, and to previously acquired AOSLO images[21] (where available) using blood vessel shadows as landmarks. The location of the fovea was marked on the AOSLO montage, based on the subject's fixation recorded in the Cirrus HD-OCT line scan ophthalmoscope image. All AOSLO images are displayed on the linear intensity scale.

To examine longitudinal changes (approximately 2 years elapsed) in the cone mosaic, previously identified areas of normal cone density were reanalyzed in subjects KS_0600 and KS_0601. At 3 locations in each subject, confocal AOSLO images from both time points were first aligned manually and then registered with rigid translations, using the Stackreg plugin from ImageJ (National Institutes of Health, Bethesda, MA) and finally cropped to the region of overlap. Cones were identified with a previously described semi-automated algorithm.[28] Cone density was calculated within 80×80 μm regions of interest (ROI).

To determine the effect of retinal lesions on the photoreceptor mosaic, the cone density was measured inside and outside macular lesions in all subjects. Because nonwaveguiding or misaligned photoreceptors are not visualized by confocal AOSLO,[27,29] split-detector AOSLO images were chosen for analysis instead. 80×80 μm ROIs were identified and analyzed for cone density across the entire span of AOSLO imaging in each subject. An ROI was characterized as intralesional if any of the ROI fell within the limits of the lesion as visualized by *en-face* OCT segmented at the level of the ellipsoid zone; then each lesion was sampled with 5 to 7 ROI to evaluate for local density variations. Cell locations within the split-detector images were identified manually. The distance between each ROI and the fovea was estimated, and cone densities were

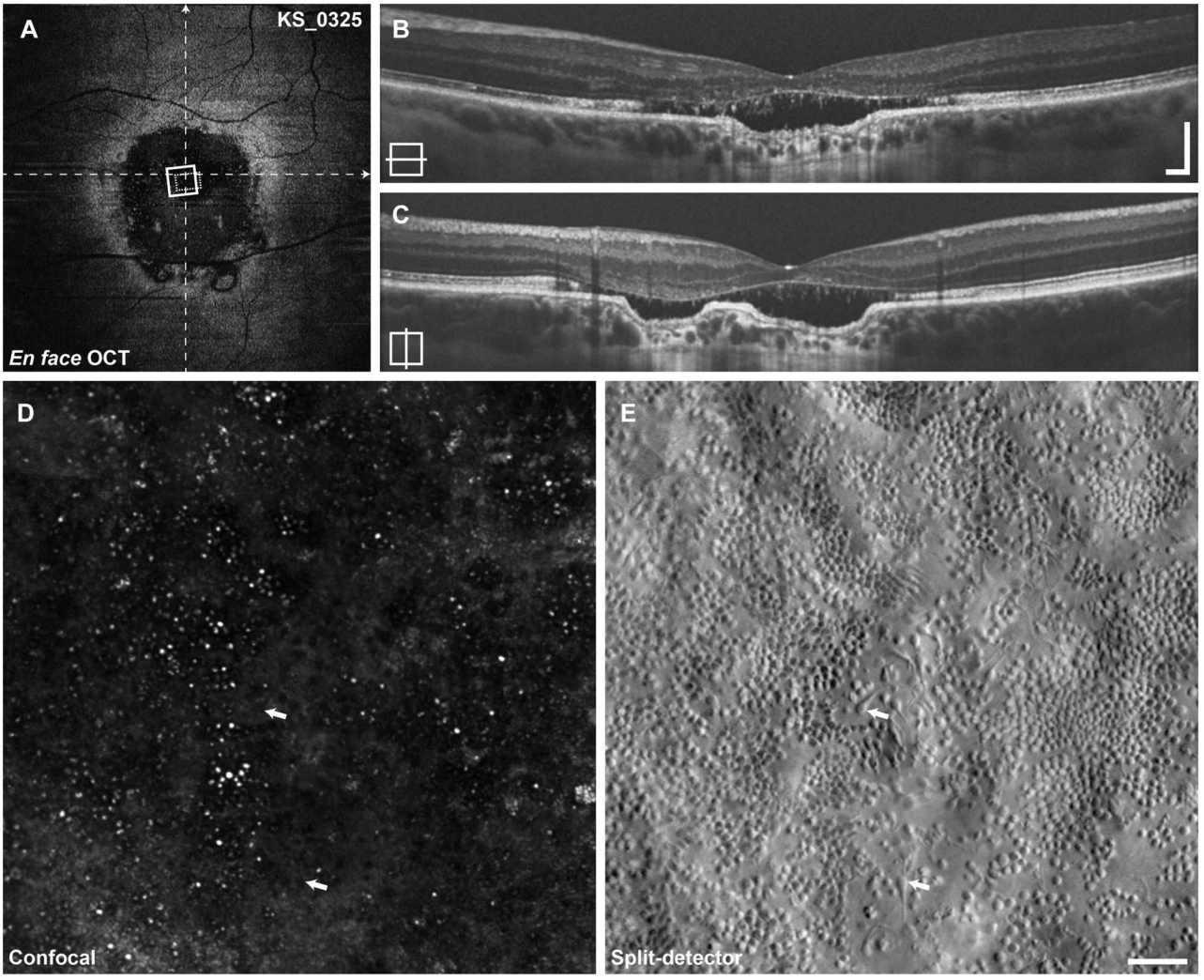

Fig. 2. Imaging results from subject KS_0325. **A.** *En-face* OCT at the level of the ellipsoid zone reveals a very large BVMD lesion with irregular borders, approximately 2.3 mm in diameter. The area of AOSLO imaging shown in (**B** and **C**) is indicated by the white square, dashed lines indicate the locations of the B-scans, and dotted rectangle indicates location of Figure 5, **A** and **B**. **B** and **C.** Horizontal and vertical B-scan OCT reveals a large atrophic lesion including the entire perifovea centered just inferior to the fovea. **D.** Confocal AOSLO imaging reveals clusters of photoreceptor reflectivity. **E.** Split-detector AOSLO reveals numerous photoreceptors in an incomplete mosaic. Most photoreceptors have abnormal morphology, and some appear to be oriented horizontally, with corresponding areas in the confocal images darker than the background (arrows). Scale bars (**B** and **C**) 200 μm, (**D** and **E**) 50 μm.

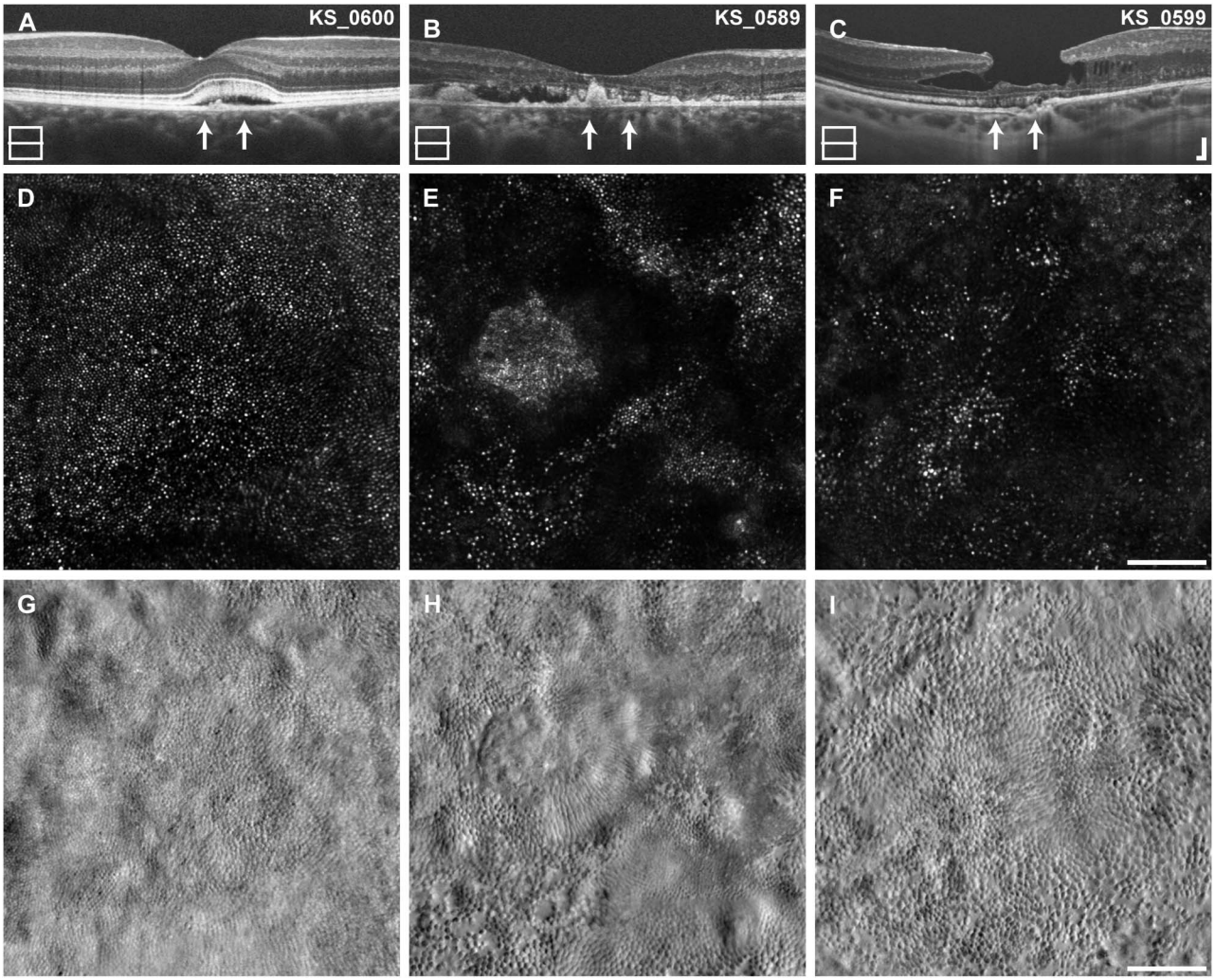

Fig. 3. Parafoveal photoreceptor imaging in remaining subjects. **A–C.** B-scan OCT, (**D–F**), confocal AOSLO imaging, and (**G–I**), split-detector AOSLO. The earliest lesion of this cohort, from KS_0600, manifests as scattered loss of waveguiding in the confocal image. The split-detector image shows a complete and normally dense mosaic of photoreceptors. The B-scan from subject KS_0589 reveals a large late vitelliruptive lesion with significant subretinal debris. The confocal AOSLO image reveals scattered waveguiding photoreceptors, with a cluster of small reflective dots on top of the large debris (**E**). The split-detector image reveals abnormal photoreceptor morphology and widely varying photoreceptor size over this small area. The bottom left corner of the image contains enlarged photoreceptors with local clearings. With this modality, it does not appear that the debris is covered by photoreceptors as the confocal image suggests. Despite the obvious retinal atrophy and little ellipsoid zone reflectivity in subject KS_0599, the split-detector AOSLO image reveals a near-complete mosaic of photoreceptors at the fovea. The confocal AOSLO image fails to identify many of the photoreceptors, likely due to their abnormal waveguiding. Scale bars 100 μm.

compared with published normative in vivo values.[30] Normative data were linearly interpolated to cover the range of measurement locations. Patient data were pooled across eccentricity for comparison, because there is no measured difference between temporal and nasal meridians across the eccentricities studied,[31–33] and superior and inferior retinal loci are likely to underestimate cone photoreceptor density.[31,32] Density data were evaluated using z-scores, calculated as the difference between the subject measurement and the normative mean divided by the standard deviation at that eccentricity. Z-scores of magnitude <2.0 were considered normal, P values < 0.05 were considered significant.

Results

The subjects included in this study had the same disease causing mutation in *BEST1* and demonstrated different stages of BVMD, with split-detector AOSLO providing unprecedented views of the photoreceptor pathology (Figures 1–3). Early in the disease, the photoreceptor mosaic remains contiguous but with substantially decreased density (Figures 1 and 3A). Later, after further cell loss has taken place, the photoreceptor packing no longer appears contiguous (Figures 2, 3, B and C). Figure 3 shows the span of photoreceptor mosaic changes across the clinically

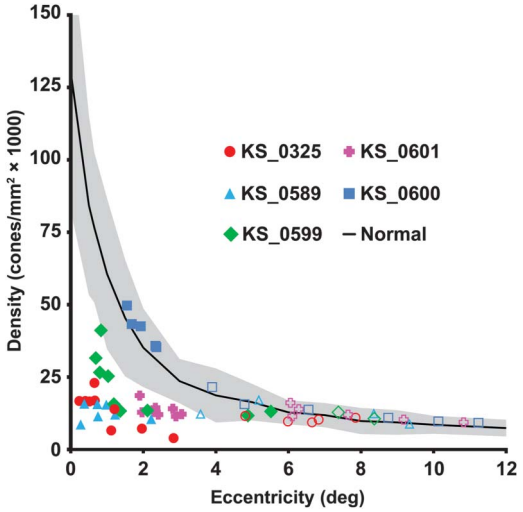

Fig. 4. Cone photoreceptor density inside and outside lesions. Density was sampled in all subjects within (filled symbols) and outside their BVMD lesion (open symbols). Cone density is significantly reduced within the lesions, but returns to normal outside lesions. Normative data[30] are shown as mean (solid line) ± two SD (shaded region).

described pathology[1] of subjects in this study from early vitelliform lesion to late-stage atrophy and fibrosis.

In all subjects, the effect of the BVMD lesion on overlying photoreceptors was assessed by comparing photoreceptor density within and outside lesions (Figure 4). Intralesion cone density was significantly reduced in subjects KS_0325, KS_0589, and KS_0601 (z-scores: −5.0 to −2.5). Near the fovea, KS_0599 exhibited reduced density (z-scores: −5.0 to −3.6), but returned to normal at the edges of the lesion (z-scores: −1.5 to −0.6). Intralesion density in subject KS_0600 was preserved (z-scores: 0.1–0.7). Extralesion cone density was near normal in all subjects (z-scores: −1.6 to 1.6) with the exception of one measurement in KS_0589 (z-score: −2.0). Within a lesion, the cone density and cone appearance varied considerably over short distances, with some regions having almost no photoreceptors, as shown in Figure 2.

Only KS_0600 and KS_0601 showed clear disease progression in OCT B-scan over 32 months and 30 months, respectively (See **Figure, Supplemental Digital Content 1** http://links.lww.com/IAE/A496, which shows longitudinal OCTs for all subjects). To determine the effect of lesion enlargement on photoreceptor number, previously analyzed areas were recounted. Three extralesional locations were analyzed in 2 subjects, at approximately 1° from the fovea and just nasal to the BVMD lesion, where cone density was previously determined to be normal.[21] In KS_0601, the cone density was found to change −2.4%, −1.7%,

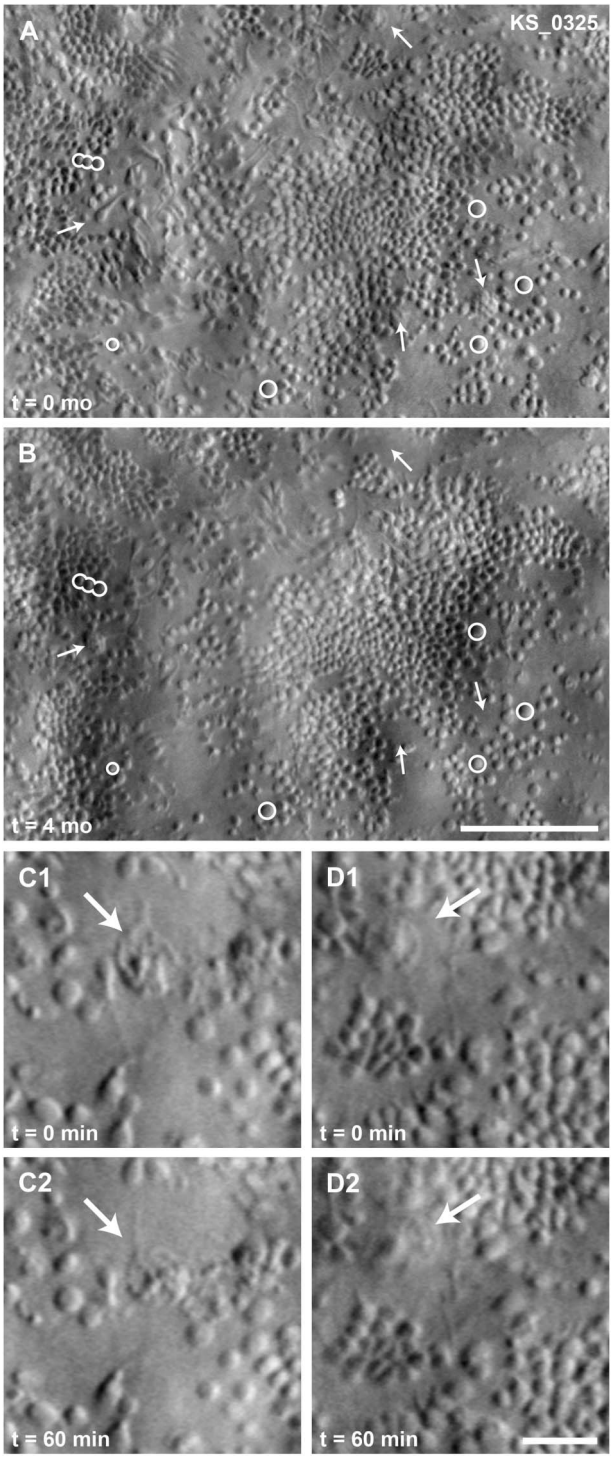

Fig. 5. Short-term and long-term variability in photoreceptor layer imaging with split-detector AOSLO in KS_0325 near the fovea center. Circles indicate photoreceptor landmarks identified in both time points. Arrows indicate features that changed over long (**A** and **B**) or short (**C1–2**, **D1–2**) time scales. Images (**C1–2**, **D1–2**) depict mobile features of size consistent with cells (arrows). Note how feature moves away from the stationary arrow between (**C1** and **C2**) and toward the arrow between (**D1** and **D2**). The cell in (**C1–2**) is visible at the top edge of (**A**) (arrow), the cell in (**D1–2**) is located approximately 200 μm temporal from (**A**). **A** and **B.** Scale bar 100 μm. **C1–2** and **D1–2.** Scale bar 25 μm.

and 1.2% over a period of 30 months. In KS_0600, the cone density was found to change 0.0%, 0.5%, and −2.6% over a period of 32 months. These small variations in cone density are within the 95% confidence interval for the repeatability of the method of parafoveal density measurements (2.6%–2.8%)[28] and are, therefore, consistent with no significant changes.

Split-detector AOSLO imaging within BVMD lesions is repeatable, even in subjects with advanced retinal degeneration as illustrated by the ability to track individual cells, shown in Figure 5. Here, the same clusters of photoreceptors were visualized over 4 months follow-up. There were, however, structures that appeared and disappeared from the images over this time scale (arrows, Figure 5). These round features had a lumpy appearance, were on average 20 μm in diameter, and appeared in areas that previously contained isolated photoreceptors or apparently empty space. Structures of similar size and appearance were also found to change in appearance on much shorter time scales, as short as an hour. These features were only noted in KS_0325, the subject with the most advanced disease.

Conclusions

Accurate assessment of cellular structure in inherited retinal degenerations in vivo can provide invaluable information about the pathology of these degenerations. In this study, we used newly developed split-detector AOSLO to further assess photoreceptor structure associated with BVMD in 5 individuals with the same previously reported *BEST1* mutation (p.Arg218Cys). Compared with confocal imaging, nonconfocal split-detector AOSLO allows for a more accurate assessment of photoreceptor structure in BVMD, especially in areas of the photoreceptor mosaic overlying subretinal pathology (Figures 1–3 and see **Figure, Supplemental Digital Content 2**, http://links.lww.com/IAE/A497, which shows split-detector and OCT imaging within and outside vitelliform lesions).

Cone photoreceptor packing within vitelliform lesions can range from normal appearing mosaic (Figure 3, D and G) to significant disruption (Figure 2). As highlighted in patients KS_0589 and KS_0599 (Figure 3), significant intralesional variability also exists with focal areas of near-normal density present next to areas with severe disruption. In the fibrotic stages of BVMD as seen in KS_0325, cone photoreceptors remain, although sparsely packed and with focal areas entirely devoid of photoreceptors (Figures 2 and 5). We hypothesize that this loose packing allows some photoreceptors to freely pivot so that they are oriented horizontally, allowing visualization of both inner and outer segments of the photoreceptors (Figure 2—teardrop shaped structures in split-detector image). This irregular packing underscores the need for caution when reporting cone photoreceptor densities within areas of pathology as visualized by AOSLO, as these can vary dramatically, even if measurements are taken within 100 μm of each other.

It has been long debated whether BVMD has only focal clinically apparent fundus effects or is a true panretinal photoreceptor disorder. The results presented here show that within clinically apparent lesions, cone photoreceptor inner segments are enlarged and cone density is reduced. In agreement with previous AOSLO studies,[21] immediately adjacent to the lesions, both density and appearance of cone inner segments return to normal (Figure 4 and see **Figure, Supplemental Digital Content 2**, http://links.lww.com/IAE/A497, which shows split-detector and OCT imaging within and outside vitelliform lesions), lending support to BVMD causing focal photoreceptor lesions. Interestingly, patient KS_0325 has been followed clinically for 5 years with the imaged lesion exhibiting detachment of the retina from the RPE over this span. Despite this change, split-detector AOSLO confirms photoreceptors overlying these lesions still exist, and combined with stable fixation within the lesions, suggests an alternate pathway for maintenance of the photoreceptors viability than from the RPE alone.

Split-detector imaging also revealed mobile disk-like structures consistent in size with cells (Figure 5, C and D). Previous histological studies have hypothesized that these cells represent subretinal macrophages,[14,34] but their lineages were not rigorously confirmed. Alternative explanations for these cells include migratory microglia[35] and RPE.[36] The significance of this finding is unknown, but these may represent the first in vivo images of reactive subretinal cells in a human eye.

Recent work by Milenkovic et al[37] suggests that the shared mutation identified in all participants in this study may affect volume-regulated anion channels in the RPE differently than other *BEST1* mutations. Although the individuals imaged represent the spectrum of stages of BVMD, the clinical and subclinical phenotypes described here cannot necessarily be extended to other mutations in *BEST1*. Conversely, the diverse findings displayed above are more likely related to the stage of the disease rather than differential pathophysiology.

In summary, the improved resolution possible with split-detector AOSLO allows for increased understanding of cellular disease processes and could potentially be useful in monitoring therapeutic response on a cellular level in diseases such as BVMD. Future studies

should be expanded to include high-resolution imaging in individuals with other mutations in *BEST1* to further explore the genotype–phenotype correlations in photoreceptor morphology in BVMD.

Key words: adaptive optics, genetics, imaging, photoreceptor, retina.

References

1. Blodi CF, Stone EM. Best's vitelliform dystrophy. Ophthalmic Paediatr Genet 1990;11:49–59.
2. Gass JDM. Best's Disease. Stereoscopic Atlas of Macular Diseases: A Funduscopic and Angiographic Presentation. St. Louis, MO: C. V. Mosby Co.; 1997:304–311.
3. Boon CJ, van den Born LI, Visser L, et al. Autosomal recessive bestrophinopathy: differential diagnosis and treatment options. Ophthalmology 2013;120:809–820.
4. Petrukhin K, Koisti MJ, Bakall B, et al. Identification of the gene responsible for Best macular dystrophy. Nat Genet 1998; 19:241–247.
5. Stone EM, Nichols BE, Streb LM, et al. Genetic linkage of vitelliform macular degeneration (Best's disease) to chromosome 11q13. Nat Genet 1992;1:246–250.
6. Marmorstein AD, Marmorstein LY, Rayborn M, et al. Bestrophin, the product of the Best vitelliform macular dystrophy gene (VMD2), localizes to the basolateral plasma membrane of the retinal pigment epithelium. Proc Natl Acad Sci U S A 2000;97:12758–12763.
7. Sun H, Tsunenari T, Yau KW, Nathans J. The vitelliform macular dystrophy protein defines a new family of chloride channels. Proc Natl Acad Sci U S A 2002;99:4008–4013.
8. Fischmeister R, Hartzell HC. Volume sensitivity of the bestrophin family of chloride channels. J Physiol 2005;562:477–491.
9. Rosenthal R, Bakall B, Kinnick T, et al. Expression of bestrophin-1, the product of the VMD2 gene, modulates voltage-dependent Ca2+ channels in retinal pigment epithelial cells. FASEB J 2006;20:178–180.
10. Arden GB, Constable PA. The electro-oculogram. Prog Retin Eye Res 2006;25:207–248.
11. Cross HE, Bard L. Electro-oculography in Best's macular dystrophy. Am J Ophthalmol 1974;77:46–50.
12. Mullins RF, Oh KT, Heffron E, et al. Late development of vitelliform lesions and flecks in a patient with best disease: clinicopathologic correlation. Arch Ophthalmol 2005;123: 1588–1594.
13. O'Gorman S, Flaherty WA, Fishman GA, Berson EL. Histopathologic findings in Best's vitelliform macular dystrophy. Arch Ophthalmol 1988;106:1261–1268.
14. Weingeist TA, Kobrin JL, Watzke RC. Histopathology of Best's macular dystrophy. Arch Ophthalmol 1982;100:1108–1114.
15. Bakall B, Radu RA, Stanton JB, et al. Enhanced accumulation of A2E in individuals homozygous or heterozygous for mutations in BEST1 (VMD2). Exp Eye Res 2007;85:34–43.
16. Zhang Y, Stanton JB, Wu J, et al. Suppression of Ca2+ signaling in a mouse model of Best disease. Hum Mol Genet 2010;19:1108–1118.
17. Kay CN, Abramoff MD, Mullins RF, et al. Three-dimensional distribution of the vitelliform lesion, photoreceptors, and retinal pigment epithelium in the macula of patients with best vitelliform macular dystrophy. Arch Ophthalmol 2012;130: 357–364.
18. Ferrara DC, Costa RA, Tsang S, et al. Multimodal fundus imaging in Best vitelliform macular dystrophy. Graefes Arch Clin Exp Ophthalmol 2010;248:1377–1386.
19. Pianta MJ, Aleman TS, Cideciyan AV, et al. In vivo micropathology of Best macular dystrophy with optical coherence tomography. Exp Eye Res 2003;76:203–211.
20. Querques G, Regenbogen M, Soubrane G, Souied EH. High-resolution spectral domain optical coherence tomography findings in multifocal vitelliform macular dystrophy. Surv Ophthalmol 2009;54:311–316.
21. Kay DB, Land ME, Cooper RF, et al. Outer retinal structure in best vitelliform macular dystrophy. JAMA Ophthalmol 2013; 131:1207–1215.
22. Abramoff MD, Mullins RF, Lee K, et al. Human photoreceptor outer segments shorten during light adaptation. Invest Ophthalmol Vis Sci 2013;54:3721–3728.
23. Glybina IV, Frank RN. Localization of multifocal electroretinogram abnormalities to the lesion site: findings in a family with Best disease. Arch Ophthalmol 2006;124:1593–1600.
24. Duncker T, Greenberg JP, Ramachandran R, et al. Quantitative fundus autofluorescence and optical coherence tomography in best vitelliform macular dystrophy. Invest Ophthalmol Vis Sci 2014;55:1471–1482.
25. Caldwell GM, Kakuk LE, Griesinger IB, et al. Bestrophin gene mutations in patients with Best vitelliform macular dystrophy. Genomics 1999;58:98–101.
26. Scoles D, Flatter JA, Cooper RF, et al. Assessing photoreceptor structure associated with ellipsoid zone disruptions visualized with optical coherence tomography. Retina 2016;36:91–103.
27. Scoles D, Sulai YN, Langlo CS, et al. In vivo imaging of human cone photoreceptor inner segments. Invest Ophthalmol Vis Sci 2014;55:4244–4251.
28. Garrioch R, Langlo C, Dubis AM, et al. Repeatability of in vivo parafoveal cone density and spacing measurements. Optom Vis Sci 2012;89:632–643.
29. Carroll J, Kay DB, Scoles D, et al. Adaptive optics retinal imaging–clinical opportunities and challenges. Curr Eye Res 2013;38:709–721.
30. Wilk MA, McAllister JT, Cooper RF, et al. Relationship between foveal cone specialization and pit morphology in albinism. Invest Ophthalmol Vis Sci 2014;55:4186–4198.
31. Curcio CA, Sloan KR, Kalina RE, Hendrickson AE. Human photoreceptor topography. J Comp Neurol 1990;292:497–523.
32. Song H, Chui TY, Zhong Z, et al. Variation of cone photoreceptor packing density with retinal eccentricity and age. Invest Ophthalmol Vis Sci 2011;52:7376–7384.
33. Zhang T, Godara P, Blanco ER, et al. Variability in human cone topography assessed by adaptive optics scanning laser ophthalmoscopy. Am J Ophthalmol 2015;160:290–300 e291.
34. Zhang Q, Small KW, Grossniklaus HE. Clinicopathologic findings in Best vitelliform macular dystrophy. Graefes Arch Clin Exp Ophthalmol 2011;249:745–751.
35. Gupta N, Brown KE, Milam AH. Activated microglia in human retinitis pigmentosa, late-onset retinal degeneration, and age-related macular degeneration. Exp Eye Res 2003;76: 463–471.
36. Zanzottera EC, Messinger JD, Ach T, et al. The project MACULA retinal pigment epithelium grading system for histology and optical coherence tomography in age-related macular degeneration. Invest Ophthalmol Vis Sci 2015;56:3253–3268.
37. Milenkovic A, Brandl C, Milenkovic VM, et al. Bestrophin 1 is indispensable for volume regulation in human retinal pigment epithelium cells. Proc Natl Acad Sci U S A 2015;112:E2630–E2639.